Correction

APPLIED BIOLOGICAL SCIENCES

Correction for "An algorithm-based topographical biomaterials library to instruct cell fate," by Hemant V. Unadkat, Marc Hulsman, Kamiel Cornelissen, Bernke J. Papenburg, Roman K. Truckenmüller, Gerhard F. Post, Marc Uetz, Marcel J. T. Reinders, Dimitrios Stamatialis, Clemens A. van Blitterswijk, and Jan de Boer, which appeared in issue 40, October 4, 2011, of *Proc Natl Acad Sci USA* (108:16565–16570; first published September 26, 2011; 10.1073/pnas.1109861108).

The authors note that Anne E. Carpenter and Matthias Wessling should be added to the author list between Roman K. Truckenmüller and Gerhard F. Post. Anne E. Carpenter should be credited with analyzing data. Matthias Wessling should be credited with designing research. The corrected author and affiliation lines, and author contributions appear below. The online version has been corrected.

Hemant V. Unadkat[a], Marc Hulsman[b], Kamiel Cornelissen[c], Bernke J. Papenburg[a], Roman K. Truckenmüller[a], Anne E. Carpenter[d], Matthias Wessling[e], Gerhard F. Post[c], Marc Uetz[c], Marcel J. T. Reinders[b], Dimitrios Stamatialis[f], Clemens A. van Blitterswijk[a], and Jan de Boer[a]

[a]Department of Tissue Regeneration, MIRA Institute for Biomedical Technology and Technical Medicine, University of Twente, 7500AE, Enschede, The Netherlands; [b]Delft Bioinformatics Lab, Delft University of Technology, Mekelweg 4, Delft, The Netherlands; [c]Department of Discrete Mathematics and Mathematical Programming, University of Twente, 7500AE, Enschede, The Netherlands; [d]Imaging Platform, Broad Institute of Harvard and MIT, Cambridge, MA 02142; [e]Membrane Science and Technology, MIRA Institute for Biomedical Technology and Technical Medicine, University of Twente, 7500AE, Enschede, The Netherlands; and [f]Department of Biomaterials Science and Technology, MIRA Institute for Biomedical Technology and Technical Medicine, University of Twente, 7500AE, Enschede, The Netherlands

Author contributions: H.V.U., M.H., B.J.P., R.K.T., M.W., G.F.P., M.U., M.J.T.R., D.S., C.A.v.B., and J.d.B. designed research; H.V.U., M.H., K.C., B.J.P., and R.K.T. performed research; H.V.U., M.H., K.C., R.K.T., A.E.C., G.F.P., M.J.T.R., D.S., C.A.v.B., and J.d.B. analyzed data; and H.V.U., M.H., K.C., B.J.P., R.K.T., M.U., M.J.T.R., D.S., and J.d.B. wrote the paper.

www.pnas.org/cgi/doi/10.1073/pnas.1204360109

Corrections

APPLIED BIOLOGICAL SCIENCES

Correction for "An algorithm-based topographical biomaterials library to instruct cell fate," by Hemant V. Unadkat, Marc Hulsman, Kamiel Cornelissen, Bernke J. Papenburg, Roman K. Truckenmüller, Anne E. Carpenter, Matthias Wessling, Gerhard F. Post, Marc Uetz, Marcel J. T. Reinders, Dimitrios Stamatialis, Clemens A. van Blitterswijk, and Jan de Boer, which appeared in issue 40, October 4, 2011, of *Proc Natl Acad Sci USA* (108: 16565–16570; first published September 26, 2011; 10.1073/pnas.1109861108).

The authors note that the following statement should be added to the Acknowledgments: "This work was supported in part by NIH Grant R01 GM089652 (A.E.C.)."

www.pnas.org/cgi/doi/10.1073/pnas.1302919110

EVOLUTION

Correction for "Diversification of rhacophorid frogs provides evidence for accelerated faunal exchange between India and Eurasia during the Oligocene," by Jia-Tang Li, Yang Li, Sebastian Klaus, Ding-Qi Rao, David M. Hillis, and Ya-Ping Zhang, which appeared in issue 9, February 26, 2013, of *Proc Natl Acad Sci USA* (110:3441–3446; first published February 11, 2013; 10.1073/pnas.1300881110).

The authors note that, within the author line, "Yang Li[a,c]" should instead appear as "Yang Li[b,c]". The corrected author line appears below. The online version has been corrected.

Jia-Tang Li[a,b], Yang Li[b,c], Sebastian Klaus[d], Ding-Qi Rao[a], David M. Hillis[e], and Ya-Ping Zhang[a,f]

www.pnas.org/cgi/doi/10.1073/pnas.1304031110

IMMUNOLOGY

Correction for "Integrity of the AID serine-38 phosphorylation site is critical for class switch recombination and somatic hypermutation in mice," by Hwei-Ling Cheng, Bao Q. Vuong, Uttiya Basu, Andrew Franklin, Bjoern Schwer, Jillian Astarita, Ryan T. Phan, Abhishek Datta, John Manis, Frederick W. Alt, and Jayanta Chaudhuri, which appeared in issue 8, February 24, 2009, of *Proc Natl Acad Sci USA* (106:2717–2722; first published February 5, 2009; 10.1073/pnas.0812304106).

The authors note that the National Institutes of Health Grant AI31541 should instead appear as AI077595.

www.pnas.org/cgi/doi/10.1073/pnas.1303069110

IMMUNOLOGY

Correction for "Alternative end-joining catalyzes robust IgH locus deletions and translocations in the combined absence of ligase 4 and Ku70," by Cristian Boboila, Mila Jankovic, Catherine T. Yan, Jing H. Wang, Duane R. Wesemann, Tingting Zhang, Alex Fazeli, Lauren Feldman, Andre Nussenzweig, Michel Nussenzweig, and Frederick W. Alt, which appeared in issue 7, February 16, 2010, of *Proc Natl Acad Sci USA* (107:3034–3039; first published January 25, 2010; 10.1073/pnas.0915067107).

The authors note that the National Institutes of Health Grant AI031541 should instead appear as AI077595.

www.pnas.org/cgi/doi/10.1073/pnas.1303073110

IMMUNOLOGY

Correction for "Downstream class switching leads to IgE antibody production by B lymphocytes lacking IgM switch regions," by Tingting Zhang, Andrew Franklin, Cristian Boboila, Amy McQuay, Michael P. Gallagher, John P. Manis, Ahmed Amine Khamlichi, and Frederick W. Alt, which appeared in issue 7, February 16, 2010, of *Proc Natl Acad Sci USA* (107:3040–3045; first published February 1, 2010; 10.1073/pnas.0915072107).

The authors note that the National Institutes of Health Grant AI031541 should instead appear as AI077595.

www.pnas.org/cgi/doi/10.1073/pnas.1303075110

IMMUNOLOGY

Correction for "Robust chromosomal DNA repair via alternative end-joining in the absence of X-ray repair cross-complementing protein 1 (XRCC1)," by Cristian Boboila, Valentyn Oksenych, Monica Gostissa, Jing H. Wang, Shan Zha, Yu Zhang, Hua Chai, Cheng-Sheng Lee, Mila Jankovic, Liz-Marie Albertorio Saez, Michel C. Nussenzweig, Peter J. McKinnon, Frederick W. Alt, and Bjoern Schwer, which appeared in issue 7, February 14, 2012, of *Proc Natl Acad Sci USA* (109:2473–2478; first published January 30, 2012; 10.1073/pnas.1121470109).

The authors note that the National Institutes of Health Grant AI031541 should instead appear as AI077595.

www.pnas.org/cgi/doi/10.1073/pnas.1303078110

An algorithm-based topographical biomaterials library to instruct cell fate

Hemant V. Unadkat[a], Marc Hulsman[b], Kamiel Cornelissen[c], Bernke J. Papenburg[a], Roman K. Truckenmüller[a], Anne E. Carpenter[d], Matthias Wessling[e], Gerhard F. Post[c], Marc Uetz[c], Marcel J. T. Reinders[b], Dimitrios Stamatialis[f], Clemens A. van Blitterswijk[a], and Jan de Boer[a,1]

[a]Department of Tissue Regeneration, MIRA Institute for Biomedical Technology and Technical Medicine, University of Twente, 7500AE, Enschede, The Netherlands; [b]Delft Bioinformatics Lab, Delft University of Technology, Mekelweg 4, Delft, The Netherlands; [c]Department of Discrete Mathematics and Mathematical Programming, University of Twente, 7500AE, Enschede, The Netherlands; [d]Imaging Platform, Broad Institute of Harvard and MIT, Cambridge, MA 02142; [e]Membrane Science and Technology, MIRA Institute for Biomedical Technology and Technical Medicine, University of Twente, 7500AE, Enschede, The Netherlands; and [f]Department of Biomaterials Science and Technology, MIRA Institute for Biomedical Technology and Technical Medicine, University of Twente, 7500AE, Enschede, The Netherlands

Edited* by Robert Langer, Massachusetts Institute of Technology, Cambridge, MA, and approved August 23, 2011 (received for review July 7, 2011)

It is increasingly recognized that material surface topography is able to evoke specific cellular responses, endowing materials with instructive properties that were formerly reserved for growth factors. This opens the window to improve upon, in a cost-effective manner, biological performance of any surface used in the human body. Unfortunately, the interplay between surface topographies and cell behavior is complex and still incompletely understood. Rational approaches to search for bioactive surfaces will therefore omit previously unperceived interactions. Hence, in the present study, we use mathematical algorithms to design nonbiased, random surface features and produce chips of poly(lactic acid) with 2,176 different topographies. With human mesenchymal stromal cells (hMSCs) grown on the chips and using high-content imaging, we reveal unique, formerly unknown, surface topographies that are able to induce MSC proliferation or osteogenic differentiation. Moreover, we correlate parameters of the mathematical algorithms to cellular responses, which yield novel design criteria for these particular parameters. In conclusion, we demonstrate that randomized libraries of surface topographies can be broadly applied to unravel the interplay between cells and surface topography and to find improved material surfaces.

high-throughput screening | microfabrication | mesenchymal stromal cells

Biomaterials are applied for numerous clinical applications, ranging from stents, orthopaedic implants, and sutures to contact lenses. In all these cases, the response of the human body to the material depends on the interface between the material and the cells. Often, interaction is not optimal. For instance, orthopaedic implants may get encapsulated by fibrous tissue upon implantation, rather than bonding directly with the bone, which can result in implant failure. Hence, a lot of effort is dedicated to modify the surface of implants by either using coatings [e.g., using calcium phosphate coatings (1) on hip implants] or through physically modifying the surface of the implant by varying the surface roughness [e.g., by sand blasting and electropolishing (2)]. Considerable improvement of orthopaedic implant performance in the past decades signifies the potential of surface modification for optimizing medical devices in general. One of the drawbacks of these techniques is that they offer only limited control of surface characteristics. However, with the advent of new developments in micro- and nanotechnologies, it is possible to create surfaces with precisely designed feature sizes and shapes up to nanometer resolution. Some of the pioneering manuscripts in the field did not only provide proof-of-principle for micro- and nanopatterning of biomaterial surfaces but also disclosed unprecedented control of material surface on the behavior of cells growing on them (3, 4). For instance, using different concentrations of poly(2-hydroxyethyl methacrylate), Folkman and Moscona were able to control cell proliferation through the extent of cell spreading (5). Using micro pattering techniques, Chen and coworkers showed that the decision of a mesenchymal stromal cell (MSC) to either become a fat or a bone cell depends on the shape the cell, which correlated with the activation of the RhoA signaling pathway (6). Micro- and nanotechnology can also be used to determine surface topography, a parameter that is known to influence the behavior of cells growing on it (7). Micrometer-range patterning is used to align cells on biomaterial surfaces (8–10), whereas Dalby et al. reported that randomly placed nanotopographies were able to induce osteogenic differentiation of MSCs (11). Unfortunately, nature does not prescribe the optimal surface topography for a given biomedical application, and the number of possible surface patterns that can be created is virtually unlimited, considering that cells are in the order of tens of micrometers whereas patterns can be created at nanometer resolution. The underlying mechanisms defining the interplay of cells with substrates are only partially understood (12–15). Additionally, the specific application of a biomedical device dictates the optimal surface as, e.g., an orthopaedic implant requires a different biological response than a cardiovascular stent. Determining the distinct surface to elicit an appropriate biological response is thus a big challenge. Due to this complex interplay between cells and substrates, rational approaches may omit unperceived paradigms (16). Hence, in recent years, there has been a shift from the rational design of biomaterials to combinatorial screening approaches used typically in the pharmaceutical industry for drug discovery, which we and others refer to as materiomics (17, 18). Thus, materiomics can be defined as large scale study of structure, function, and properties of natural and synthetic materials. In a landmark study, Anderson et al. identified a host of unexpected material effects that offered new levels of control over human embryonic stem cell behavior while evaluating an array of nearly 600 different copolymer compositions (16). In this manuscript, we show that combining the power of high-throughput screening with mathematical design of micrometer-range surface topographies, enables deciphering the "Braille code" of cell-topography interactions.

Author contributions: H.V.U., M.H., B.J.P., R.K.T., M.W., G.F.P., M.U., M.J.T.R., D.S., C.A.v.B., and J.d.B. designed research; H.V.U., M.H., K.C., B.J.P., and R.K.T. performed research; H.V.U., M.H., K.C., R.K.T., A.E.C., G.F.P., M.J.T.R., D.S., C.A.v.B., and J.d.B. analyzed data; and H.V.U., M.H., K.C., B.J.P., R.K.T., M.U., M.J.T.R., D.S., and J.d.B. wrote the paper.

Conflict of interest statement: Jan de Boer, Bernke Papenburg, and Clemens van Blitterswijk are shareholders of Materiomics B.V., which commercializes the TopoChip platform.

*This Direct Submission article had a prearranged editor.

Freely available online through the PNAS open access option.

[1]To whom correspondence should be addressed. E-mail: j.deboer@utwente.nl.

This article contains supporting information online at www.pnas.org/lookup/suppl/doi:10.1073/pnas.1109861108/-/DCSupplemental.

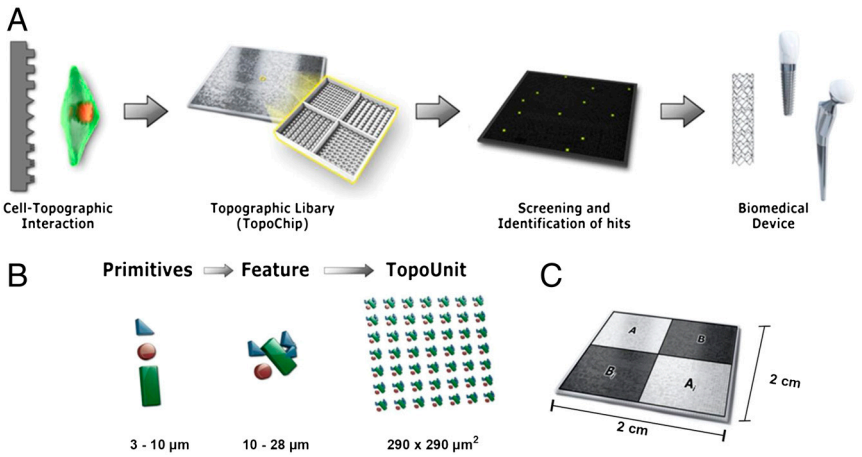

Fig. 1. TopoChip design. (*A*) A schematic representation of a sequence of events that is proposed to be followed for high-throughput screening of biomedical materials starting from initial design to clinical application. (*B*) Design of the TopoChip is based on the use of primitives. Three types of primitives, namely circles, triangles, and lines were used to construct features. Repeated features constitute a TopoUnit and two times 2,176 = 4,352 TopoUnits constitute a TopoChip (size ranges are indicated). In addition, four flat control surfaces are included. (*C*) TopoChip is divided into four quadrants. TopoUnits in quadrant A are repeated in quadrant A_i and similarly TopoUnits in quadrant B are repeated in quadrant B_i in order to exclude site specific or localized effects.

Results

We created a library of 2,176 distinct, randomly designed surface topographies using mathematical algorithms as a design tool (see Fig. 1*A* for an outline). They were reproduced in duplicate on a 2 by 2 cm^2 chip ("TopoChip") from poly(DL-lactic acid) (PLA) in areas of 290 by 290 μm^2, designated as "TopoUnits" (see Fig. 1*B*). First, a library of surface topographies was designed by generating topographic features, which are topography containing elements with a height of 5 μm arranged within an imaginary square with a size of either 10 by 10, 20 by 20, or 28 by 28 μm^2 (Fig. 1*B*). Topographic features are built up using three types of microscale primitive shapes: circles, isosceles triangles (with one angle of 36° and two angles of 72°), and thin rectangles (3 μm width). We choose these shapes because by combining these primitives, we can generate different types of patterns—e.g., circles can create large smooth areas, triangles can generate angles, and thin rectangles can result in stretched elements. With integral values for geometrical parameters (see Tables S1 and S2) such as primitive type, primitive size, and angle of rotation in the algorithm, 154,320,600 possible surface topographies can be defined. If we include nonintegral values for these parameters, the possibilities are infinite. From the in silico library, 2,176 topographic designs were randomly selected. In addition, four TopoUnits with a flat, nonpatterned surface were included as reference surfaces. We divided the TopoChip into four quadrants (Fig. 1*C*) where quadrant A has identical TopoUnits to that of A_i and quadrant B is identical to quadrant B_i to assure that TopoUnits at the periphery have duplicates in the middle of the chip (Fig. 1*C*). With the TopoChip design, a silicon mould was fabricated using photolithography and etching, which was then used for imprinting of topographies onto PLA films. The chips were diced and further characterized using scanning electron microscopy (SEM; Fig. 2 *A* and *B*). Upon characterization, we observed uniformity in the filling of the polymer into the mould cavities spaces. To assess the accuracy of replication of topographies, 32 TopoUnits were randomly chosen and height profile measurements of them performed using a Keyence VK9700 confocal laser scanning microscope. It is important to note that the chips used in this study were composed of features with a height of 5 μm and 20-μm-high walls between adjacent TopoUnits (Fig. S1). For each location, the measurements were performed on three chips. The average difference in height profile measurements was 99 nm with a standard deviation of 56 nm. TopoChips can also be coated with different materials used in tissue engineering. In Fig. S2, TopoChips are displayed with a layer of titanium oxide, deposited using plasma sputtering, and a calcium phosphate coating deposited using supersaturated simulated body fluids. Thus, we created a library of thousands of surfaces with unique physicochemical compositions.

Cell Seeding and Culture. To analyze the bioactivity of topographies, primary human mesenchymal stromal cells (hMSCs) were seeded onto PLA TopoChips and cell-material interaction was analyzed by high-content imaging. We anticipated that quantification of cell behavior relies on a critical number of cells per TopoUnit. Cell seeding has to be homogenous across the chip and the seeding density needs to be controlled. To this end, we designed and

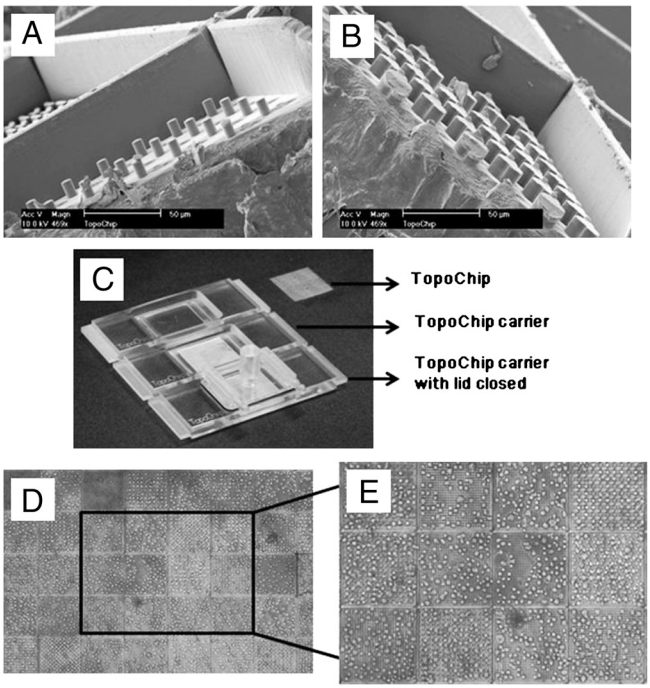

Fig. 2. TopoChip fabrication and characterization. (*A* and *B*) SEM images of sections of TopoChips, displaying accurate feature replication on the TopoChip. (Scale bar: 50 μm.) (*C*) The TopoChip carrier, lid, and chip assembly. This chip carrier can even be used as a micro-bioreactor for perfusion culture of cells, or with a second set of attachment (not shown) for static cell culture. (*D* and *E*) Light microscopic images of cells seeded using the chip carrier displaying homogeneity of cell distribution within and between TopoUnits.

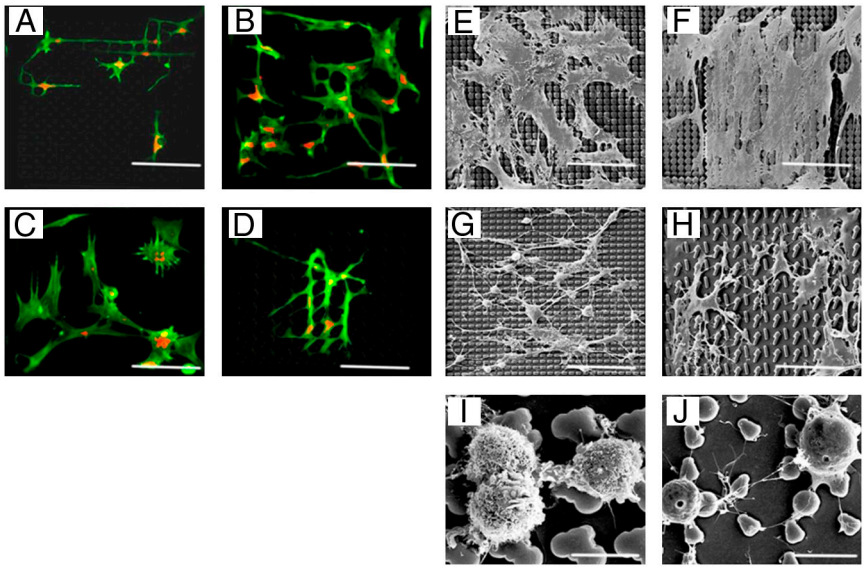

Fig. 3. Morphology of hMSCs on different TopoUnits. (*A–D*) Fluorescent microscopic images of spread and elongated cells showing alignment on topographic features (pseudocolored green: actin stained with Alexa Fluor 488 phalloidin; red: nuclear staining with TOTO-3; scale bar: 90 μm). (*E–H*) SEM images of cells showing diverse cellular morphologies. (Scale bar: 90 μm.) (*I* and *J*) High magnification SEM images of rounded cells on two distinct TopoUnits showing differences in the texture of cell membrane. (Scale bar: 10 μm.)

fabricated a chip carrier by micromachining poly(methylmethacrylate) (Fig. 2*C*) to retain the chip in position. Design and quality control aspects of TopoChip seeding and the culturing device will be described in a separate manuscript. The chip carrier was fabricated with a removable closing lid that can be fixed within a slot which is placed 100 μm above the chip. Homogeneous distribution of the cell suspension across the chip area was observed upon closure of the lid and the cells were deposited into the TopoUnits by gravity (Fig. 2 *D* and *E*). To confirm that the topographic features affect hMSC behavior, we fixed the cells 8 h after seeding and stained their actin cytoskeleton. Visual inspection of the chip confirmed that a multitude of different cellular morphologies were induced by surface topography (Fig. 3 *A–J*). For instance, TopoUnits were found in which hMSCs adopted an elongated shape, or in which cells spread extensively, but also TopoUnits were seen in which the hMSCs remained mostly rounded. In many TopoUnits, cells exhibited extensive filopodia, and many cells were observed that clearly followed the outlines of the features.

Mitogenic Effect of Surface Topographies. To quantitatively screen for surface topographies that can exert a mitogenic effect on hMSCs, we seeded the cells, synchronized the cell cycle by serum deprivation and treated the cells with the nucleoside analogue EdU at the moment that serum was added to the cells. After 8 h of culture with serum, cells were stained for EdU and nuclei were stained with TOTO-3. Fluorescent images of the nuclei, proliferating nuclei and bright field images of TopoUnits were acquired for the whole chip area using an automated microscope. A preprocessing pipeline was designed in which the images were corrected for background and signal intensity distribution and quality control metrics were calculated in order to remove unreliable results (Fig. S3). The images obtained from preprocessing were analyzed using a CellProfiler pipeline (19), which was used to count the total number of cells per TopoUnit as well as the number of proliferating cells per unit, represented by the number of EdU-positive cells. To improve reliability, the experiment was repeated five times, giving us for each of the 2,176 units ten measurements (two per chip, $n = 10$). In Fig. 4*A*, the average number of cells per TopoUnit is represented. Similarly, the average number of EdU-positive cells is represented in a heat map (Fig. S4), which clearly shows that large differences occur between different TopoUnits confirming that surface topography influences cell proliferation (20). Finally, we analyzed the number of EdU-positive cells per total cell number per TopoUnit (Fig. 4*B*). The surface patterns of top scoring units in terms of the number of proliferating cells are shown in Fig. S4 *C–F*. Because all cells in the TopoChip share the same 5 ml of medium in the reservoir, it is possible that the biological response is not a direct effect of

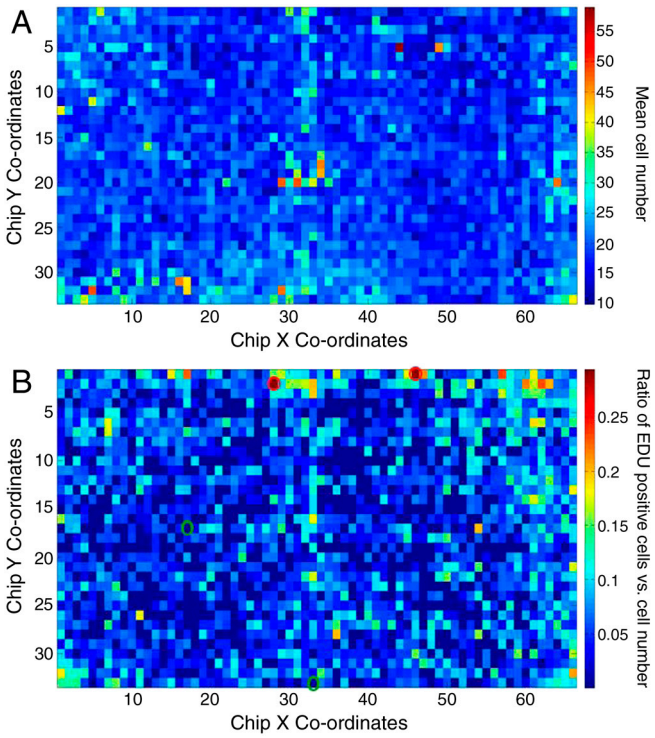

Fig. 4. Cell proliferation assay. (*A*) Heat map of the mean cell number per TopoUnit. The numbers represent the average of 10 TopoUnits on five TopoChips ($n = 10$). (*B*) Heat map of the ratio of the mean number of proliferating cells over total cell number. TopoUnits marked with red circles indicate high-scoring units in terms of cell proliferation ratio. Flat TopoUnits (without any features) are indicated with green circles.

the surface topography but rather mediated through short-range signals produced by cells in adjacent units. Under these circumstances, a "colony" of positive TopoUnits would be expected, which we did not observe in the heat maps. Furthermore, it is not very likely that the small numbers of cells in the TopoUnit are able to create a morphogen gradient in such a large volume of medium. However, to represent the extent to which the surface topography itself is predictive of class fate (proliferating or nonproliferating), we trained a nearest-neighbor classifier (21) (see *Materials and Methods*) to distinguish between high- and low-scoring TopoUnits based on surface topography parameters using the highest and lowest 10% of the observations. The classifier was employed in a 10-fold cross-validation setting, in which it was trained with a subset of the TopoUnits, and afterwards used to predict the outcome of another subset of TopoUnits. By comparing predictions with the actual measurements, an area under curve score (AUC) (22) from the receiver operating characteristics (ROC) curve (see *Materials and Methods*) of 0.68 (Fig. 5*A*) was obtained, confirming that surface topography correlates to the proliferation of hMSCs, and thus mitogenicity depends on surface topography.

Machine Learning Algorithms for Identification of Important Topographic Parameters. At first sight, no apparent common design theme could be observed between the four topographic features that stimulate cell proliferation (Fig. S4 *C–F*). To gain more insight in which (combination) of the 35 topographic parameters was most influential in determining proliferation, we performed a forward parameter selection. For this, a classifier algorithm was trained using only a subset of topographic parameters to distinguish between TopoUnits with high and low numbers of proliferating cells. This was again done for the 10% highest vs. 10% lowest measurements. The classifier was tested using a cross-validation strategy to give us an estimation of the predictive power of subsets of topographic parameters. As shown in Fig. 5*B*, we found that the best single parameter predictive of the number of proliferating cells was the Fourier-based parameter WN1 (AUC = 0.67). Performance improved even further when forward selection included WN1.5 along with feature size and WN1 (AUC = 0.70). The parameters WN1.5 and WN1 represent the fraction of the total energy contained in the feature after applying discrete Fourier transformation that is present in sinusoids with wave number approximately 1.5 and 1, respectively. These observations suggest that cell proliferation can be triggered by concentrating on designs that are composed of a certain spatial distribution.

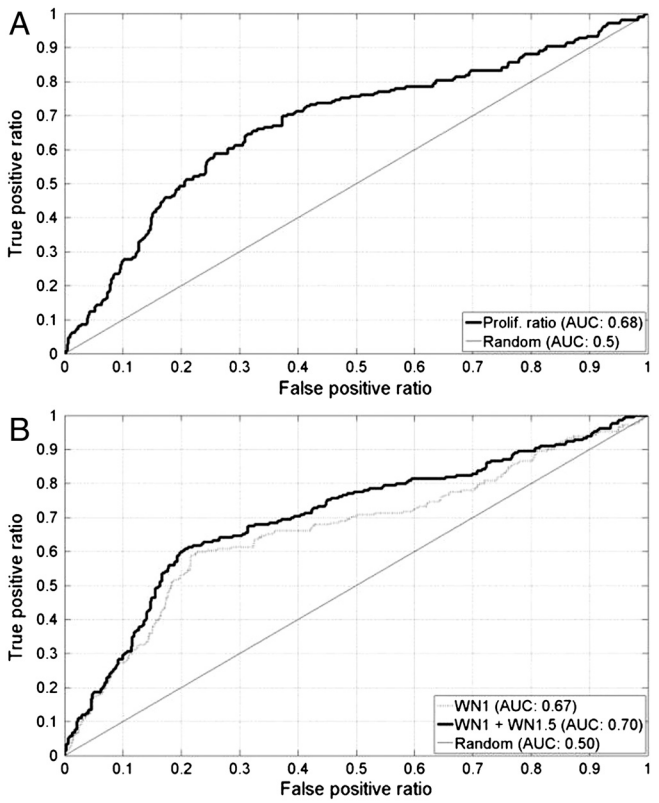

Fig. 5. Data validation for the cell proliferation assay. (*A*) ROC curve to rule out stochastic events for validation of proliferating cell count ratio as a function of surface topography after tenfold cross-validation. (*B*) ROC curve to determine surface topographic parameters responsible for enhanced proliferation with a machine-learnt model.

Surface Topography Enhances Osteogenic Differentiation of hMSCs. High-content screening of TopoChips can be performed using virtually any fluorescence-based cellular staining. To further illustrate this, we analyzed the expression of alkaline phosphatase (ALP), a marker for early osteogenic differentiation, using hMSCs growing in basic medium on TopoChips. It has been shown in the past that surface topography is able to induce osteogenic differentiation in the absence of growth factors (11). Following cell culture, the cells were stained by immunofluorescence using a bone-specific antihuman ALP antibody. Immunofluorescence images of chips were acquired and ALP intensity was analyzed using CellProfiler software. First of all, we detected ALP-positive cells in less than 10% of the TopoUnits. Fig. 6*A* represents mean ALP signal measured across five chips ($n = 10$) , and immunofluorescent staining of hMSCs on the flat control is shown in Fig. 6*B*. The TopoUnit with the highest average/mean ALP intensity across 10 measurements is shown in Fig. 6 *C* and *D*. It has been reported that cell shape can influence osteogenic differentiation, and cell spreading seems to correlate positively to osteogenic differentiation (6). To investigate whether cell spreading was also related to ALP expression in our hit surfaces, we analyzed the morphology of hMSCs on the top hit surface and flat reference surfaces using CellProfiler software (see Table 1). Of the 13 parameters analyzed, cells on the hit surface displayed a significantly smaller cell area and a higher major axis length. Osteogenic differentiation is known to be enhanced in more compact three-dimensional structures, such as nodules or spheroids (23) and the area of the ALP-positive MSCs on the high-scoring surface could be related to this, which is currently under investigation.

Discussion

Taken together, our data confirm the viability of a previously undescribed approach to address the problem of unknown biological responses to a virtually unlimited number of potential surface pattern designs. In this manuscript, we have combined algorithmic generation of surface topographies with high-throughput screening of hMSCs, aiming at the identification of bioactive surface topographies.

An important pillar of the study is the use of high-content imaging and assay miniaturization. The current TopoChip contains 2,176 unique surface topographies, which we were able to screen and analyze simultaneously. Typically, research on the effect of surface topography on cell behavior is characterized by low throughput, with some notable exceptions (24, 25). Although exact calculations are difficult to make, we think that more unique surface patterns were screened for an effect on proliferation and osteogenic differentiation of hMSCs in this manuscript alone than ever published in literature. As such, we believe TopoChip screening can lead to a paradigm shift in research on surface topography, not only because of the throughput but also because our approach is based on the design of the surfaces. The current TopoChip comprises features down to a few micrometers, but

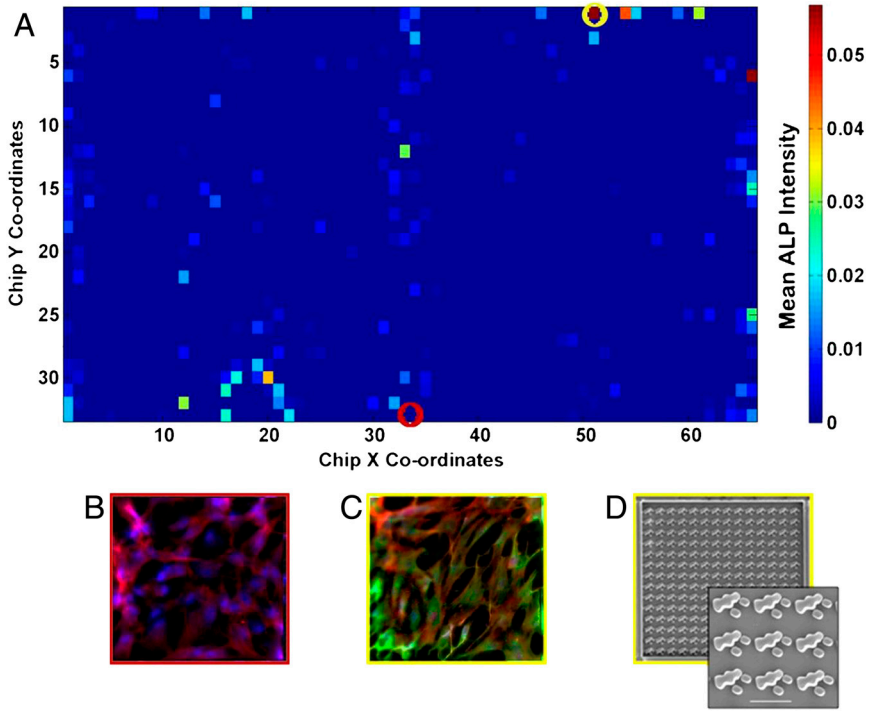

Fig. 6. ALP expression on hMSCs. (*A*) Heatmap of the mean intensity of fluorescently labeled ALP of hMSCs grown on different topographies. (*B*) Cells on/in a flat TopoUnit not expressing any ALP. In this image, actin staining is pseudocolored in red, ALP expression in green, and nucleic acid staining in blue. (*C*) Cells on the TopoUnit with the highest ALP expression. The corresponding TopoUnit is marked with a yellow circle on the heat map. (*D*) SEM image of the TopoUnit showing the highest intensity for ALP staining. The inset shows a higher magnification view of features. (Scale bar: 20 μm.)

future work will also focus on fabrication of TopoChips with nanometer scale topographic features, where the interaction with the cells may lead to yet another level of control.

Another powerful aspect of the TopoChip platform is its versatility. We used it to screen biological responses that are useful in bone regeneration strategies—i.e., hMSC proliferation and differentiation—but the platform can be used with different materials and cell types as well. For example, we have initiated experiments to screen for surfaces that support embryonic stem cell pluripotency, for surfaces that are favorable for proliferation of endothelial cells and surfaces with antiadhesive properties for bacteria to prevent biofilm formation (26). With a well-defined biomaterial and biological readout, straightforward screening projects for a myriad of different medical devices can be envisaged.

Beyond the use of TopoChip technology as a biomaterial development tool, we think it will also be instrumental in shedding new light on the scientific questions around the interplay between surface topography and cell behavior. It is well recognized that cells respond to the surface they sit on, or in other words, we do know that cells can read a "Braille language" and respond to it. Analogous to the six simple dots that are enough to encode the Braille alphabet, it would be very interesting to decode the cell's Braille script. How many unique cellular responses can be evoked by virtue of surface topography and what are the molecular mechanisms behind it? The algorithmic approach we used in the current study is particularly suited for this enterprise because the biological response can be correlated to design criteria of the materials. For instance, we did not anticipate that hMSC proliferation would correlate to the Fourier transform of certain features, a mathematical description of the spatial organization of topographic features on the surface (27). To fully explore the potential of this approach, systematic development of methodologies is needed that allows for generations of favorable surface topographies in environments with unpredictable response. This asks for development of new tools and insights in the design of (evolutionary) search algorithms, requires pushing the limits in imaging and nanoscale fabrication technologies, and most importantly, calls for a carefully designed hybrid of algorithmic and biological experiments. For instance, we are currently developing a nanoTopoChip for which e-beam lithography will be used, and we already produced TopoChips of various compositions including hydrogels. Moreover, we are developing the TopoChip into a device that is compatible with six-well plates in order to make the technology more accessible for other research groups and to be able to screen even larger numbers of different TopoUnits. We believe that incorporation of iterative experimental and bioinformatics-based computational approaches for studying bio-

Table 1. CellProfiler analysis of hMSCs on a flat versus a hit surface*

Parameter	Flat surface	Hit surface	P value†
Area	2868‡	2333	0.009
Compactness	1.45	1.51	0.06
Eccentricity	0.77	0.78	0.26
Center X	221	231	0.37
Center Y	222	225	0.39
Euler no.	0.898	0.809	0.52
Extent	0.507	0.511	0.76
Form factors	0.235	0.227	0.47
Major axis length	78.9	84.2	0.004
Minor axis length	43.4	48.2	0.06
Orientation	−19.2	6.4	0.09
Perimeter	431	388	0.18
Solidity	0.76	0.75	0.25

*Cell profiler parameters were selected describing cell shape and measured in the flat reference surfaces and the hit surface with the highest ALP intensity.
†Student's *t* test on the average parameter values.
‡On three TopoChips, about 40–50 cells were imaged per indicated TopoUnit. Average numbers are represented.

materials will help us better understand cell–material interactions and develop better surfaces for medical devices.

Materials and Methods

Design and Fabrication. As mentioned previously, topographies were designed using three types of primitive shapes—i.e., triangles, circles, and rectangles. A feature was generated by first randomly selecting parameter values for its size, the number of primitives to be used and the distribution over the different primitive types, the size of the primitives, and the degree to which the primitives were to be aligned. Next, each primitive was placed at a random position inside the feature. Overlapping of primitives was allowed.

After designing the chip, a chromium mask was made and used for photolithography. The micro patterns were etched from the silicon wafer, generating a silicon master for hot embossing. To render a hydrophobic mould surface for easier demoulding, the master was coated with a layer of perfluorodecyltrichlorosilane (FDTS) (ABCR, AB111155) in an evacuated recipient. The master was subsequently used for hot embossing of PLA films (250 μm thick) (Folienwerk Wolfen GmbH) using an Obducat nanoimprint tool. Briefly, the silicon master was placed at the bottom and the PLA film was sandwiched between the silicon master and an Obducat UV Sheet Polyester (100 Micron 10638). Imprinting was carried out at 80 °C with 30 bars of pressure for 10 min and then the assembly was allowed to cool down to 40 °C prior to demoulding. The chips were diced from the imprinted PLA films using a wafer saw.

Cell Culture. HMSCs were isolated from a healthy donor and expanded as described previously (28). Briefly, cells were expanded in proliferation medium containing α-MEM (Gibco, 22-571-038), 10% foetal bovine serum (FBS; Lonza), 2 mM L-glutamine (Gibco, 25030), 0.2 mM ascorbic acid (Sigma, A8960), 100 U/mL penicillin + 100 g/ml streptomycin (Gibco, 15140-122) and 1 ng/mL basic fibroblast growth factor (bFGF; Instruchemie, PhP105). For the cell proliferation assay, hMSCs were trypsinised using 0.25% trypsin-EDTA (Invitrogen 25200-072), resuspended in basic medium (proliferation medium devoid of bFGF) and treated with Component A from a Click-iT™ EdU Alexa Fluor® 488 Imaging Kit (C10083) according to manufacturer's protocol. For immunofluorescence staining of ALP, cells were resuspended in basic medium to a concentration of 1.2 million cells per millilitre and seeded on the chips. The cells were cultured in a humid 5% CO_2 environment.

Immunofluorescence Staining. After cell culture, the chips were washed with phosphate buffered saline and cells were fixed with 4% (w/v) paraformaldehyde for 10 min and permeabilized with 0.01% Triton X-100. Staining for EdU detection was performed using the EdU imaging kit according to manufacturer's protocol and cells were counterstained with TOTO-3 iodide nucleic acid stain (Invitrogen, T3604) according to manufacturer's protocol. For ALP detection, following permeabilization cells were incubated with a solution of 10% FBS for nonspecific antibody blocking and stained for ALP using a bone-specific human ALP antibody (developmental study hybridoma bank B4-78). The cells were counterstained with Alexa Fluor 568 phalloidin (Invitrogen, A12380) and TOTO-3 iodide.

Image Acquisition and Analysis. Images were acquired using a BD Pathway 435 automated microscope. A montage of a total of 221 montage images with respective filter sets for each fluorophore was acquired. Each image constituted a 3 by 5 montage of an area covering approximately 20 TopoUnits. All the 221 montage images were combined into one large montage (35,000 by 35,000 pixels) for each channel and corrected for rotation, overlap, and intensity. Focus performance was determined using a Laplace operator and unreliable measurements were discarded. Subsequently, images of individual TopoUnits were cropped and analyzed using CellProfiler. For details see Fig. S3.

Data Analysis. To distinguish high-scoring TopoUnits from low-scoring ones, a nearest-neighbor classifier was applied. This is a method for classifying objects based on closest training examples (TopoUnits) in the (surface topography) parameter space and is widely used in the field of signal processing and pattern recognition. To determine classifier performance, a 10-fold cross-validation strategy was employed, and ROC curves were constructed. ROC curves are a widely used standard for describing and comparing the accuracy of diagnostic tests. It represents the trade-off between the true and false positive rates for every possible classifier threshold. For each ROC curve, the AUC was determined, which is a measure of the probability that a classifier based on this label would rank a randomly chosen positive observation (e.g., enhanced proliferation) higher than a randomly chosen negative observation. AUC = 1 is a perfect ranking classifier and AUC = 0.5 depicts complete randomness.

1. Habibovic P, Barrere F, van Blitterswijk CA, de Groot K, Layrolle P (2002) Biomimetic hydroxyapatite coating on metal implants. *J Am Ceram Soc* 85:517–522.
2. Meredith DO, Eschbach L, Riehle MO, Curtis ASG, Richards RG (2007) Microtopography of metal surfaces influence fibroblast growth by modifying cell shape, cytoskeleton, and adhesion. *J Orthop Res* 25:1523–1533.
3. Huebsch N, et al. (2010) Harnessing traction-mediated manipulation of the cell/matrix interface to control stem-cell fate. *Nat Mater* 9:518–526.
4. Lutolf MP, Blau HM (2009) Artificial stem cell niches. *Adv Mater* 21:3255–3268.
5. Folkman J, Moscona A (1978) Role of cell shape in growth control. *Nature* 273:345–349 (Translated from English).
6. McBeath R, Pirone DM, Nelson CM, Bhadriraju K, Chen CS (2004) Cell shape, cytoskeletal tension, and RhoA regulate stem cell lineage commitment. *Dev Cell* 6:483–495.
7. Ratner BD, Bryant SJ (2004) Biomaterials: Where we have been and where we are going. *Annu Rev Biomed Eng* 6:41–75.
8. Papenburg BJ, et al. (2007) One-step fabrication of porous micropatterned scaffolds to control cell behavior. *Biomaterials* 28:1998–2009.
9. Curtis A, Wilkinson C (1997) Topographical control of cells. *Biomaterials* 18:1573–1583.
10. Bettinger CJ, Orrick B, Misra A, Langer R, Borenstein JT (2006) Micro fabrication of poly (glycerol-sebacate) for contact guidance applications. *Biomaterials* 27:2558–2565.
11. Dalby MJ, et al. (2007) The control of human mesenchymal cell differentiation using nanoscale symmetry and disorder. *Nat Mater* 6:997–1003.
12. Stevens MM, George JH (2005) Exploring and engineering the cell surface interface. *Science* 310:1135–1138.
13. Lutolf MP, Gilbert PM, Blau HM (2009) Designing materials to direct stem-cell fate. *Nature* 462:433–441.
14. Lecuit T, Lenne PF (2007) Cell surface mechanics and the control of cell shape, tissue patterns and morphogenesis. *Nat Rev Mol Cell Biol* 8:633–644.
15. Marklein RA, Burdick JA (2010) Controlling stem cell fate with material design. *Adv Mater* 22:175–189.
16. Anderson DG, Levenberg S, Langer R (2004) Nanoliter-scale synthesis of arrayed biomaterials and application to human embryonic stem cells. *Nat Biotechnol* 22:863–866.
17. Mei Y, et al. (2008) Cell-compatible, multicomponent protein arrays with subcellular feature resolution. *Small* 4:1600–1604.
18. Flaim CJ, Chien S, Bhatia SN (2005) An extracellular matrix microarray for probing cellular differentiation. *Nat Methods* 2:119–125.
19. Carpenter AE, et al. (2006) CellProfiler: Image analysis software for identifying and quantifying cell phenotypes. *Genome Biol* 7, 10.1186/Gb-2006-7-10-R100.
20. Dalby MJ, Riehle MO, Johnstone HJH, Affrossman S, Curtis ASG (2002) Polymer-demixed nanotopography: Control of fibroblast spreading and proliferation. *Tissue Eng* 8:1099–1108.
21. Cover TM, Hart PE (1967) Nearest neighbor pattern classification. *IEEE T Inform Theory* 13:21–27.
22. Hanley JA, Mcneil BJ (1982) The meaning and use of the area under a receiver operating characteristic (roc) curve. *Radiology* 143:29–36.
23. Kale S, et al. (2000) Three-dimensional cellular development is essential for ex vivo formation of human bone. *Nat Biotech* 18:954–958.
24. Lovmand J, et al. (2009) The use of combinatorial topographical libraries for the screening of enhanced osteogenic expression and mineralization. *Biomaterials* 30:2015–2022.
25. Markert LD, et al. (2009) Identification of distinct topographical surface microstructures favoring either undifferentiated expansion or differentiation of murine embryonic stem cells. *Stem Cells Dev* 18:1331–1342.
26. Statz AR, Meagher RJ, Barron AE, Messersmith PB (2005) New peptidomimetic polymers for antifouling surfaces. *J Am Chem Soc* 127:7972–7973.
27. Assender H, Bliznyuk V, Porfyrakis K (2002) How surface topography relates to materials' properties. *Science* 297:973–976.
28. Both SK, van der Muijsenberg AJ, van Blitterswijk CA, de Boer J, de Bruijn JD (2007) A rapid and efficient method for expansion of human mesenchymal stem cells. *Tissue Eng* 13:3–9.